WELL-POSED EULER MODEL OF SHOCK AND DETONATION INDUCED TWO-PHASE FLOW IN BUBBLY LIQUID

R. R. Tukhvatullina[1] **and S. M. Frolov**[1,2]

[1]Center for Pulse Detonation Combustion
Moscow, Russia
[2]N. N. Semenov Institute of Chemical Physics
Russian Academy of Sciences
Moscow, Russia
e-mail: smfrol@chph.ras.ru

A well-posed mathematical model of nonisothermal two-velocity two-phase flow of bubbly liquid is proposed. The model is based on two-phase Euler equations with the inclusion of an additional pressure at the gas bubble surface, which ensures the well-posedness of the Cauchy problem for a system of governing equations with homogeneous initial conditions, and the Rayleigh–Plesset equation for radial pulsations of gas bubbles. The model is validated by comparing one-dimensional (1D) calculations of shock wave (SW) propagation in liquids with gas bubbles with a volume gas content of 0.5% to 30% with experimental data. The model is shown to provide satisfactory results for the shock propagation velocity, SW pressure profiles, and shock-induced motion of bubbly liquid column.

1 Introduction

The propogation of an SW in bubbly liquid has been the subject of numerous investigations. It is known that the initial value problem (IVP) for the system of Euler equations governing the two-velocity two-phase flow with common pressure is ill-posed [1–3]. The ill-posedness of the models based on such a system is often associated with the insufficiently detailed account for the interfacial interaction of bubbles or dispersed

particles. Various methods of problem regularization were suggested in the literature which are reported in reviews [1–3].

In this paper, a well-posed mathematical model of nonisothermal two-velocity two-phase flow of bubbly liquid is proposed. The model is based on two-phase Euler equations containing two pressures rather than one (common) pressure of phases with an additional pressure specified at the bubble–liquid interface, which ensures the well-posedness of the IVP for the system of governing equations with homogeneous initial conditions. The additional pressure is obtained using the local pressure coefficient averaged over the interface for different Reynolds numbers of relative motion of phases. The radial pulsations of bubbles are taken into account by coupling the governing equations with the Rayleigh–Plesset equation. The new model is shown to reproduce the oscillating structure of an SW propagating in bubbly liquid as observed in experiments [4–6]. The model applicability conditions are formulated, which are equivalent to those derived in [7].

2 Model

Let us consider a model of nonisothermal two-velocity two-phase bubbly medium composed of liquid as carrier phase and noncondensable gas bubbles as dispersed phase. The pressures in liquid and in gas are assumed to be connected via the Rayleigh-Plesset equation. In addition to the pressures of phases, the interphase pressure is introduced into the model to make the IVP well-posed. When formulating the governing equations, it was also assumed that interphase heat transfer was much slower than dynamic relaxation of phases. Thus, the system of governing equations is formulated as follows:

$$\left.\begin{aligned} \frac{\partial \phi_f \rho_f}{\partial t} + \nabla_k \left(\phi_f \rho_f u_f^k\right) = 0\,; \\ \frac{\partial \phi_f \rho_f u_f^j}{\partial t} + \nabla_k \left(\phi_f \rho_f u_f^k u_f^j + p_f \phi_f\right) - p_I \nabla_j \phi_f = F_f\,; \\ \frac{\partial \phi_f \rho_f E_f}{\partial t} + \nabla_k \left(\rho_f u_f^k (\rho_f E_f + p_f)\right) + p_I \frac{\partial \phi_f}{\partial t} = H_f \end{aligned}\right\} \qquad (1)$$

where index f denotes either the liquid phase (index 1) or the gas phase (index 2); and ϕ_f, u_f, p_f, ρ_f, and E_f refer to the volume fraction, velocity, pressure, density, and the total energy of phase f, respectively.

The processes in liquid phase are considered as isothermal and the energy conservation equation for phase 1 is omitted; p_I is the interfacial pressure defined as

$$p_I = p_1 + C_s\left(\phi_2, \mathrm{Re}\right)\rho_1\Delta^2\,. \tag{2}$$

Here, $\Delta = (u_1 - u_2)$; $C_s\left(\phi_2, \mathrm{Re}\right)$ is the emperical function that depends on the volume gas fraction; and $\mathrm{Re} = 2\rho_1 R\Delta/\mu_1$ is the Reynolds number where R is the mean radius of bubbles per unit volume. The volume fraction constraint reads:

$$\phi_1 + \phi_2 = 1\,. \tag{3}$$

The system of Eqs. (1) is coupled with the Rayleigh–Plesset equation describing radial motions of a bubble:

$$\left.\begin{aligned} \frac{d_2 R}{dt} &= \omega\,; \\ \rho_1 R\frac{d_2\omega}{dt} + \rho_1\frac{3}{2}\,\omega^2 &= p_2 - \frac{4\mu_1}{R}\,\omega - \frac{2\sigma}{R} - p_1 \end{aligned}\right\} \tag{4}$$

where ω is the bubble pulsation rate; μ_1 is the liquid viscosity; σ is the surface tension; and $d_2/dt = \partial/\partial t + u_2^k\nabla_k$ denotes the substantial derivative with respect to time. The oscillations of the gas bubble volume in the liquid are determined by the inertia of the added mass, phase pressure difference, and viscous dissipation. The mean bubble radius and the volume fraction are related by the formula:

$$\phi_2 = \frac{4}{3}\,\pi R^3 N \tag{5}$$

where N is the number of the gas bubbles per unit volume, which is assumed constant $N = N^0$ herein.

Assuming that the liquid is incompressible and the gas is ideal, one comes to two additional relationships closing problem formulation:

$$\rho_1 = \rho_1^0\,; \quad \rho_2 = \frac{p_2}{(\gamma - 1)e_2} \tag{6}$$

where γ is the ratio of specific heats and $e_2 = E_2 - u_2^2/2$ is the internal energy of the gas phase.

The system of Eqs. (1) to (6) is supplemented with the relations for fluxes:

$$\left.\begin{aligned} F_2^j &= -F_1^j = C_d(\mathrm{Re})\frac{A\rho_1(u_1^j - u_2^j)|u_1^j - u_2^j|}{8}\,; \\ H_2 &= -H_1 = \mathrm{Nu}\,\kappa_1\frac{A(T_1 - T_2)}{d} \end{aligned}\right\} \tag{7}$$

where T_f is the temperature of phase f; C_d is the drag coefficient; Nu is the Nusselt number; $A = 6\phi_2/d$ is the total area of interphase boundary per unit volume of bubbly liquid; $d = 2R$ is the bubble diameter; and κ_1 is the specific heat of liquid.

The method used for numerical solution of Eqs. (1)–(7) is based on the algoritm proposed in [6], but it is modified for the case of different pressures in phases.

3 Well-Posedness of the Problem

The IVP for the system (1)–(6) in the 1D case is considered under the following assumptions:

$$p_I > 0\,; \tag{8}$$

$$C_s\,(\phi_2, \mathrm{Re}) < -\phi_2\,. \tag{9}$$

In the present analysis, the problem has been simplified and algebraic terms in (1) and the surface force and the viscous term in (4) have not been considered. For convenience, radius R can be expressed by ϕ_2 using (5) in the Eqs. (4). Therefore, the system (1)–(6) is solved for $w = (\phi_2, p_2, p_1, u_2, \rho_2, w_b)^{\mathrm{T}}$.

By w_0, let denote constant initial conditions for all variables:

$$w(x, 0) = w_0\,. \tag{10}$$

Furthermore, let suppose that bubbles are in equilibrium at the initial conditions, i. e., one obtains for w_0:

$$p_2^0 = p_1^0\,; \quad w_b^0 = 0\,; \tag{11}$$

then, w_0 is the constant solution of the system.

To examine whether the evolution problem is well-posed, one has to check the continuous solution dependence on the initial conditions.

Let perturb the initial conditions (10) $w'(0,x) = w_0 + w^\delta \sin(\alpha x)$ where α is the disturbance frequencies and w^δ is the disturbance amplitude.

Linearize equations (1)–(6) in the vicinity of the constant solution w_0:

$$w(x,t) = w_0 + w'(x,t)\,. \tag{12}$$

Substitute (12) into (1)–(6), assuming that disturbance is small, i. e., let neglect terms of the second order in w'. As a result, one obtains a set of linear equations with constant coefficients (for details, see Appendix A):

$$T\frac{\partial w'}{\partial t} + A\frac{\partial w'}{\partial x} + Qw' = 0\,. \tag{13}$$

Let find the solution of (13) in the form $w' = w^\delta e^{i(\omega t+\alpha x)}$. Substituting $w' = w^\delta e^{i(\omega t+\alpha x)}$ into (13), one arrives at:

$$(i\omega T + i\alpha A + Q)w^\delta = 0\,. \tag{14}$$

Equation (14) has a nontrivial solution provided their determinant is equal to zero:

$$\left\| -\lambda T + A - \frac{i}{\alpha}\,Q \right\| = 0 \tag{15}$$

where $\lambda(\alpha) = -\omega/\alpha$ is the solution of (15). The Cauchy problem for Eqs. (1)–(6) subjected to the initial condition (10) is well-posed, if there exists a constant $\overline{c}$ such that inequality $\mathrm{Im}\,[\omega(\alpha)] \geq \overline{c}$ holds for all $\alpha \in R$.

Since $\lambda = u_2^0$ is a root, then other roots of the characteristic equation can be obtained from a fourth-degree polynomial, which can be written in the form $P_2(\lambda) = P_1(\lambda)$ (for details, see Appendix B). The polynomial $P_1(\lambda)$ has roots $\lambda_{1,2}^{(1)} = u_2^0 \pm c_2^0$ and

$$\lambda_{3,4}^{(1)} = u_2^0 + \frac{\Delta^0(\phi_2^0 \pm f(\delta))}{\delta\phi_1^0 + \phi_2^0}$$

where

$$\delta = \frac{(R^0\alpha)^2}{3}\,;$$
$$f(\delta) = \left[-C_s^0\phi_2^0 - \delta\phi_1^0(C_s^0 + \phi_2^0\right]^{1/2}\,;$$
$$C_s^0 = C_s(\phi_2^0, \mathrm{Re}^0)\,.$$

If (9) holds, then the expression under the root is nonnegative. One has $P_1(\lambda) \to +\infty$ as $\lambda \to \pm\infty$ and $\lambda_{1,2}^{(2)} = u_2^0$ are the roots of $P_2(\lambda)$. If (8) holds, then one also obtains $P_2(\lambda) \to +\infty$ as $\lambda \to \pm\infty$.

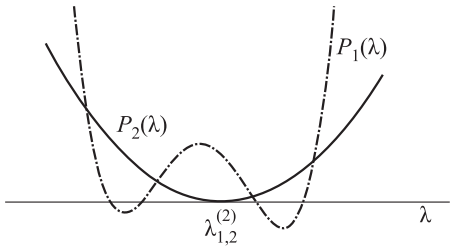

Figure 1 A graphical representation of polynomials $P_1(\lambda)$ and $P_2(\lambda)$

Let us now prove that the multiple root $\lambda_{1,2}^{(2)} = u_2^0$ of $P_2(\lambda)$ is located between the pairs of roots of $P_1(\lambda)$ as shown in Fig. 1, i. e., the corresponding curves have four intersection points and all roots of the characteristic equation (15) are real ($\mathrm{Im}\,[\omega(\alpha)] = 0$).

From the above, one has $\lambda_2^{(1)} < \lambda_{1,2}^{(2)} < \lambda_1^{(1)}$. Let denote

$$\psi_1(\delta) = \frac{\phi_2^0 - f(\delta)}{\delta\phi_1^0 + \phi_2^0};$$
$$\psi_2(\delta) = \frac{\phi_2^0 + f(\delta)}{\delta\phi_1^0 + \phi_2^0}.$$

If $\Delta^0 > 0$, then it is sufficient to show that $u_2^0 + \Delta^0\psi_1(\delta) < u_2^0 < u_2^0 + \Delta^0\psi_2(\delta)$. But from above, one has $\psi_2(\delta) > 0$. The inequality $\psi_1(\delta) < 0$ holds from (9). The case $\Delta^0 < 0$ can be cosidered similarly with the only difference that $u_2^0 + \Delta^0\psi_2(\delta) < u_2^0 < u_2^0 + \Delta^0\psi_1(\delta)$. Therefore, the system (1)–(6) with constant initial condition (10) and (11) in the 1D case under assumptions (8) and (9) is well-posed.

4 Function $C_s(\phi_2, \mathrm{Re})$

The distribution of pressure over the surface of a rigid sphere is gived by [8]:

$$p_1(\theta) = p_{1,\infty} + \frac{1}{2}\,\rho_1 R\frac{d\overline{U}_z}{dt}\cos(\theta) + \frac{1}{8}\,\rho_1 U_z^2\left(9\cos^2(\theta) - 5\right). \qquad (16)$$

When deriving Eq. (16), it is assumed that the sphere is moving along the z-axis with velocity $U = U_x e_z$ in the unconfined volume of ideal incompressible liquid. In Eq. (16), $p_{1,\infty}$ stands for the liquid pressure at a large distance from the sphere, θ for the angle between the z-axis and the radius-vector connecting the center of the sphere with a point at its surface. On the one hand, when the Reynolds number of the relative flow of phases exceeds 24, the fore/aft symmetry in the nonaccelerated component in Eq. (16) is known to be disturbed due to flow separation [7]. On the other hand, when the Reynolds number is much less than 24, then shear viscosity dominates which is not taken into account in Eq. (16). Therefore, the present authors suggest to rewrite Eq. (16) in the following form:

$$p_1(\theta) = p_{1,\infty} + \frac{1}{2}\,\rho_1 R \frac{dU_z}{dt}\cos(\theta) + \rho_1 U_z^2 F(\theta) \tag{17}$$

where function $F(\theta)$ can be obtained from the experiment based on the relation $F(\theta) = C_p(\theta)/2$ with

$$C_p(\theta) = \frac{p_1(\theta) - p_{1,\infty}}{\rho_1 \Delta^2/2}$$

usually referred to as the local pressure coefficient at point θ on the surface. In general, the local pressure coefficient depends on the Reynolds number, the shape of the body, and others parameters. If one averages Eq. (17) over the surface of the sphere (denote this operation by $\langle\cdot\rangle^s$), then

$$p_I \equiv \langle p_1\rangle^s = p_{1,\infty} + \rho_1 \Delta^2 \langle F(\theta)\rangle^s$$

where $C_s \equiv \langle F(\theta)\rangle^s$, i. e., C_s is the local pressure coefficient averaged over the sphere surface, and $\langle F(\theta)\rangle^s$ is equal to

$$\langle F(\theta)\rangle^s = \frac{1}{4\pi R^2}\int\limits_{-\pi}^{\pi} d\psi \int\limits_{0}^{\pi} \sin(\theta) F(\theta)\, d\theta = \frac{1}{4}\int\limits_{0}^{\pi} \sin(\theta) C_p(\theta)\, d\theta\,. \tag{18}$$

In [7], coefficient C_s is associated with the hydrodynamic drag coefficient C_d: $C_s = -0.37 C_d$ at Re = 163,000. However, the coefficient of proportionality (-0.37) depends on the Reynolds number, since C_s is

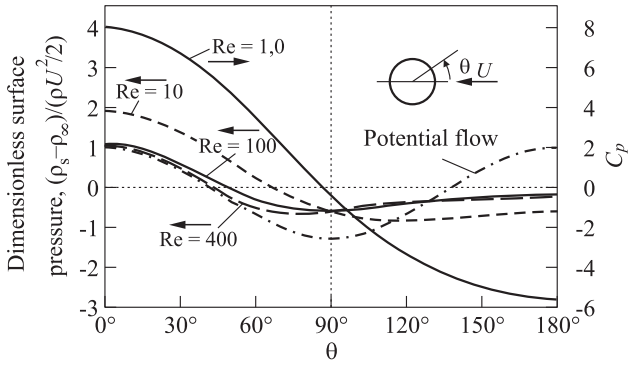

Figure 2 Distributions of $C_p(\theta)$ over the surface of a rigid sphere for different Reynolds numbers [9]

the mean value of $F(\theta)$ and C_d is the mean value of $F(\theta)\cos(\theta)$. Therefore, the present authors suggest to calculate C_s directly through the Reynolds number.

Figure 2 shows the distributions of the local pressure coefficient over the surface of a rigid sphere at different Reynolds numbers [9]. The C_p curves in Fig. 2 are obtained from numerical calculations. Substituting various $C_p(\theta)$ into Eq. (18), one obtains $\langle F(\theta)\rangle = -0.1$ for Re = 10, $\langle F(\theta)\rangle = -0.12$ for Re = 100, and $\langle F(\theta)\rangle = -0.15$ for Re = 400 and 163,000. These values can be approximated, for example, by the following function at Re $\geq$ 10:

$$C_s(\mathrm{Re}) = C_s^0 + \kappa e^{-(\mathrm{Re}-\psi)/\beta}$$

where $C_s^0 = -0.15$; $\kappa = 0.05$; $\beta = 244.21$; and $\psi = 10$.

If one considers a gas bubble instead of sphere, then coefficient C_s can be treated as the local pressure coefficient averaged over the interface surface separating liquid and gas phases. Therefore, if the Reynolds number exceeds 10 and the gas volume fraction is relatively small ($\phi_2 \leq 0.1$), the condition (9) is satisfied. If the gas volume fraction exceeds 0.1, it is necessary to take into account the collective effects of bubbles, for example, by applying relation $C_s(\phi_2, \mathrm{Re}) = C_s(\mathrm{Re})(1-\phi_2)^{-2.7}$ proposed in [7].

Since $C_s(\phi_2, \mathrm{Re}) < 0$, then it follows from Eq. (2) that pressure p_I may become negative. In this case, the model should be extended by including the cavitation phenomenon.

5 Results and Discussion

The model of section 2 was validated by comparing the results of 1D calculations of SW propagation in a bubbly liquid with experimental data [6,10]. The experiment in [10] was performed in the vertical shock tube 1980 mm long with rectangular 50×100 mm cross section. The tube was equipped with a 495-millimeter-long high-pressure gas section (HPS), a 495-millimeter-long low-pressure gas section (LPS), and a 990-millimeter-long test section (TS) filled with bubbly water to a preset level 943 mm above the end-wall with bubble generator. An SW was generated by bursting a thin diaphragm separating the HPS and the LPS. The pressure in the HPS (≈ 0.3 MPa at the time of diaphragm bursting) is obtained by supplying compressed air. The average diameter of bubbles was approximately 2.5 mm and the initial volume gas fraction ranged from 0.005 to 0.3. The water and the air were at room temperature. The pressure in the propagating pressure waves was measured by six pressure sensors. The SW velocity at different measuring segments was calculated based on the SW arrival times and the distance between the sensors. Also measured in [10] was the shock-induced velocity of the contact surface between air and bubbly water just after the SW passes through this region using high-speed video recording.

The calculations were made for different experimental conditions in terms of the initial gas volume fraction. Figure 3 compares the results of calculations with experiments for the mean SW velocity between two pressure sensors located at positions 1172 and 1440 mm counted from the top of the tube. The mean SW velocity is calculated as the ratio of the distance between the sensors to the time interval taken for the SW to travel between the sensors. The results of calculations are seen to be consistent with the experimental data. The differences between the predicted and measured SW velocities are seen to be within the measurement errors for $\phi_2^0 \geq 0.01$.

Shown in Fig. 4 is the comparison of predicted and measured contact surface velocities for different volume gas fractions under conditions of experiments in [10].

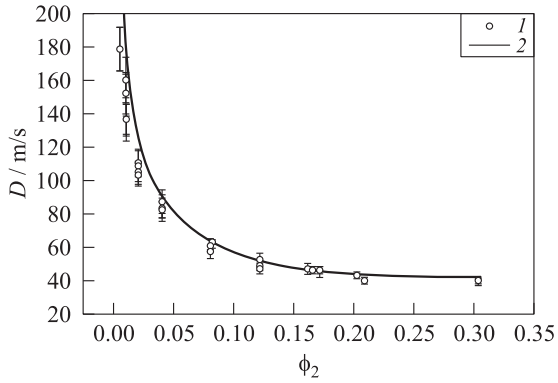

Figure 3 Comparison of predicted (curve) and measured (signs with error bars [10]) dependencies of the mean SW velocity on the gas volume fraction in bubbly water: *1* — experiment; and *2* — calculation

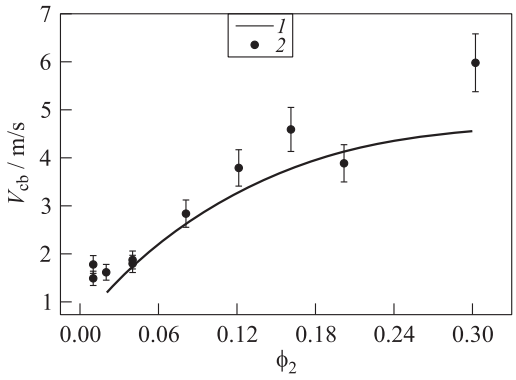

Figure 4 Comparison of predicted (curve) and measured (signs with error bars [10]) dependencies of the mean contact surface velocity on the gas volume fraction in bubbly water: *1* — experiment; and *2* — calculation

Figure 5 compares the predicted pressure profile in an SW, propagating in bubbly water with $\phi_2^0 = 0.02$ with the profile measured experimentally in [10]. Clearly, the model of section 2 predicts the oscillatory structure of the SW which is known to be caused by nonlinear

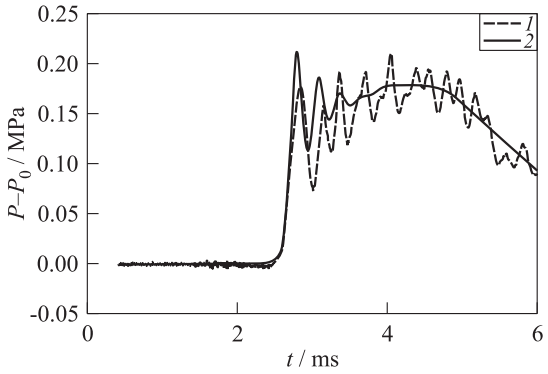

Figure 5 Comparison of predicted (solid curve) and measured in [10] (dashed curve) pressure histories in a SW penetrating bubbly water with $\phi_2^0 = 0.02$ at a preset position of pressure sensor: *1* — experiment; and *2* — calculation

and disperse properties of bubbly liquids. The predicted oscillation frequency (~ 3.7 kHz) correlates within 10% with the measured value and the amplitudes of the first few fluctuations are well consistent with the measurements. Note that subsequent pressure oscillations in the experiment can be caused by transverse motions of fluid due to pressure waves traversing the channel in transverse direction. It is also worth noting that a condition for the existance of the oscillatory pressure profiles in a weak SW with $\delta p/p_0 \ll 1$ (δp is the pressure amplitude and p_0 is the initial pressure in the medium) was obtained in [11]: if the kinematic viscosity of liquid is less than a certain critical value

$$v_{\rm cr} = \sqrt{\frac{R^2 c_0^2 \delta p}{3\phi_2^0 p_0}\,\frac{\gamma+1}{2\gamma}}$$

(here, c_0 is the isentropic speed of sound), then an SW exhibits the oscillatory structure; otherwise, its structure is monotonous.

Figure 6 compares the predicted and measured in [6] pressure profiles in a weak SW with $\delta p/p_0 \le 1$. Plotted in Fig. 6 are the pressure profiles predicted by the model of section 2 and by the model developed in [6]. The model in [6] includes simulation of motion and pulsations of

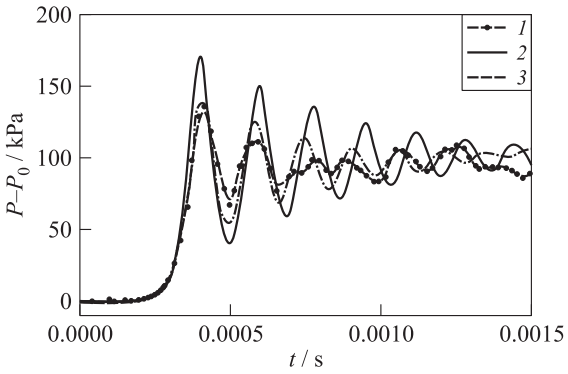

Figure 6 Comparison of predicted (curves without signes) and measured in [6] (curve with circles) pressure histories in an SW penetrating bubbly silicon oil with $\phi_2^0 = 0.0015$ at a preset position of pressure sensor: *1* — experiment; *2* — calculation; and *3* — calculation by Kameda [6]

each individual bubble in the bubbly liquid and is seen to correlate with measurements somewhat better than the present model. However, application of this model to simulation of SW phenomena in bubbly media with multiple bubbles is extremely CPU time-consuming. Thereby, the model of section 2 can be considered as a good alternative. Note that experiments in [6] were conducted at the most favorable conditions for studying the oscillatory SWs due to the use of nitrogen gas and silicone oil with high viscosity ensuring the spherical shape of bubbles and no bubble fragmentation upon interaction with the SW. The experiment was conducted in a vertical shock tube of inner diameter 18 mm. The tube was divided into three parts with a 1.6-meter-long HPS, 1.8-meter-long LPS, and a 2-meter-long TS. The data of the experiment are: $\phi_2^0 = 0.0015$; $R_0 = 0.601$ mm; $p_0 = 101.2$ kPa; $\delta p = 101.2$ kPa; and $z = 311$ mm (z is the depth of a bubbly liquid column where the pressure sensor is located).

6 Concluding Remarks

A well-posed mathematical model of nonisothermal two-velocity two-phase flow of bubbly liquid is proposed. The model is based on two-

phase Euler equations with the inclusion of an additional pressure at the gas bubble surface, which ensures the well-posedness of the Cauchy problem for a system of governing equations with homogeneous initial conditions. The additional pressure is obtained using the local pressure coefficient averaged over the phase interface for different Reynolds numbers of relative motion of phases. Radial pulsations of gas bubbles are taken into account via coupling of the governing equations with the Rayleigh–Plesset equation. The applicability conditions of the model are formulated. The model is validated by comparing 1D calculations of SW propagation in water with air bubbles with a volume gas content of 0.5% to 30% with experimental data. The model is shown to provide satisfactory results for the shock propagation velocity, SW pressure profiles, and shock-induced motion of gas bubbles in bubbly liquid.

Appendix A

$$T = \begin{pmatrix} \rho_2^0 & 0 & 0 & 0 & 0 & \alpha_2^0 & 0 \\ -1 & 0 & 0 & 0 & 0 & 0 & 0 \\ 0 & 0 & 0 & \rho_2^0\alpha_2^0 & 0 & 0 & 0 \\ 0 & 0 & 0 & 0 & \rho_1\alpha_1^0 & 0 & 0 \\ \dfrac{p^0 + (\gamma-1)p_I^0}{\alpha_2^0} & 1 & 0 & 0 & 0 & 0 & 0 \\ 1 & 0 & 0 & 0 & 0 & 0 & 0 \\ 0 & 0 & 0 & 0 & 0 & 0 & 1 \end{pmatrix};$$

$$a = \begin{pmatrix} \rho_2^0 u_2^0 & 0 & 0 & \rho_2^0\alpha_2^0 & 0 & u_2^0\alpha_2^0 & 0 \\ -u_1^0 & 0 & 0 & 0 & \alpha_1^0 & 0 & 0 \\ p^0 - p_I^0 & \alpha_2^0 & 0 & \rho_2^0 u_2^2 \alpha_2^0 & 0 & 0 & 0 \\ p_I^0 - p^0 & 0 & \alpha_I^0 & 0 & \rho_1 u_1 \alpha_1^0 & 0 & 0 \\ \dfrac{(p^0 + (\gamma-1)p_I^0)u_2^0}{\alpha_2^0} & u_2^0 & 0 & \gamma p^0 & 0 & 0 & 0 \\ u_2^0 & 0 & 0 & 0 & 0 & 0 & 0 \\ 0 & 0 & 0 & 0 & 0 & 0 & u_2^0 \end{pmatrix}$$

where $p^0 = p_2^0 = p_1^0$ and $p_I^0 = p^0 + C_s(\phi_2^0, \mathrm{Re}^0)\rho_1(u_1^0 - u_2^0)^2$. For matrix Q, there are no zero elements only for $Q_{7,2} = -1$, $Q_{7,3} = 1$, and $Q_{6,7} = -4\pi N(R^0)^2$.

Appendix B

The polynomials are written in the following form using the relations $c_2^2\rho_2 = p_2\gamma$ and Eq. (2):

$$P_1(\lambda) = \rho_2^0 \left(\chi\rho_1 \left(\lambda - u_1^0\right)^2 \phi_2^0 + \chi\rho_1 C_s \left(\phi_2^0, \mathrm{Re}^0\right) \left(\Delta^0\right)^2 + \phi_2^0\phi_1^0 \left(\lambda - u_2^0\right)^2 \right) \left(\left(\lambda - u_2^0\right)^2 - \left(c_2^0\right)^2 \right) ;$$

$$P_2(\lambda) = \chi\rho_2^0 \left(\lambda - u_2^0\right)^2 \gamma p_I^0 \left(1 - \phi_2^0\right)$$

where

$$\chi = \frac{3\phi_2^0}{(R^0\alpha)^2\rho_1} .$$

Acknowledgments

The work was supported by the Russian Ministry of Education and Science under the State Contract No. 14.609.21.0001 (Contract IDRFMEFI57914X0038).

References

1. Ramshaw, J. D., and J. A. Trapp. 1978. Characteristics, stability, and short-wavelength phenomena in two-phase flow equation systems. *Nuclear Sci. Eng.* 66(1):93–102.
2. Stewart, H. B. 1979. Stability of two-phase flow calculation using two-fluid models. *J. Comput. Phys.* 33(2):259–270.
3. Klebanov, L. A., A. E. Kroshilin, B. I. Nigmatulin, and R. I. Nigmatulin. 1982. On the hyperbolicity, stability and correctness of the Cauchy problem for the system of equations of two-velocity motion of two-phase media. *J. Appl. Math. Mech.* 46(1):66–74.
4. Noordzij, L. 1971. Shock waves in bubble-liquid mixtures. *Phys. Commun. Twente Univ. Tech.* 3(1):52.
5. Burdukov, A. P., V. V. Kuznetsov, S. S. Kutateladze, V. E. Nakoryakov, B. G. Pokusaev, and I. R. Shreiber. 1973. Shock wave in a gas–liquid medium. *J. Appl. Mech. Tech. Phys.* 14(3):349–352.
6. Kameda, M., and M. Yoichiro. 1996. Shock waves in a liquid containing small gas bubbles. *Phys. Fluids* 8(2):322–335.

7. Stuhmiller, J. H. 1977. The influence of interfacial pressure forces on the character of two-phase flow model equations. *Int. J. Multiphase Flow* 3(6):551–560.
8. Lamb, H. 1932. *Hydrodynamics*. Cambridge University Press.
9. Clift, R., J. R. Grace, and M. E. Weber. 2005. *Bubbles, drops, and particles*. Courier Corporation.
10. Avdeev, K. A., V. S. Aksenov, A. A. Borisov, R. R. Tukhvatullina, S. M Frolov, and F. S. Frolov. 2015. Chislennoe modelirovanie vozdeystviya udarnoy volny na puzyr'kovuyu sredu [Numerical modeling of the impact of shock wave on bubbly environment]. *Goren. Vzryv (Mosk.) — Combustion and Explosion* 8(2):45–56.
11. Kutateladze, S. S., and V. E. Nakoryakov. 1984. *Teplomassoobmen i volny v gazozhidkostnykh sistemakh* [Heat and mass transfer and waves in gas–liquid systems]. Novosibirsk: Nauka.